

Correspondence: Prof. P. Espinet

Room Temperature Columnar Mesophases in Triazine/Gold-Thiolate Metalorganic Supramolecular Aggregates

*Cristina Domínguez,^a Benoît Heinrich,^b Bertrand Donnio,^b Silverio Coco,^{*a} and Pablo Espinet.^{*a}*

^a IU CINQUIMA/Química Inorgánica, Facultad de Ciencias, Universidad de Valladolid, 47071 Valladolid, Castilla y León, Spain. ^b Institut de Physique et Chimie des Matériaux de Strasbourg (IPCMS), UMR 7504 (CNRS-ULP), 23 rue du Loess, BP 43, F-67034 Strasbourg Cedex 2 (France).

Abstract

Supramolecular mono and dinuclear liquid crystalline gold(I) aggregates have been synthesized by means of hydrogen bond interactions of 2,4,6-triarylamino-1,3,5-triazine with gold thiolate metalloacids $[\text{Au}(\text{PR}_3)(\text{SC}_6\text{H}_4\text{COOH})]$ or $[\mu\text{-(binap)\{Au}(\text{SC}_6\text{H}_4\text{COOH})\}_2]$, in 1:1 and 2:1 molar ratio, respectively. All the supramolecular aggregates display a stable columnar hexagonal mesophase (Col_h) at room-temperature. The supramolecular arrangement within the columns consists of the one-dimensional stacking of triazine units with the core of the attached metallic thioacid fragments acting as the fourth branch. The phosphine-containing moieties of the metallic thioacid protrude out in the aliphatic continuum. The complexes prepared here do not show metallophilic interactions but this strategy looks very promising for the future design of room-temperature LC mesophases containing interacting metallic fragments.

Introduction

Molecular self-assembly into ordered supramolecular structures offers an interesting approach to functional materials. This is the case of columnar liquid-crystalline materials combining functions derived from their columnar structure, such high charge carrier mobility along the columnar stacks,^{1,2} with those derived from the mesophase, such as anisotropy and fluidity. Materials with columnar phases can be generated from disc-like molecules, but also from species able to fill discotic spaces upon supramolecular aggregation,³ including some gold containing metallomesogens.⁴ Non-covalent interactions, such as hydrogen bonds, have been widely used to this purpose, and appropriate combination of simpler molecular units can afford discotic liquid crystals.⁵ Moreover, the reversibility of the hydrogen bonds opens the possibility of preparing dynamically functional assemblies such as catalytically active capsules,⁶ or molecular machines.⁷

Since the seminal systematic studies on the hydrogen bond dimerization of 4-alkoxybenzoic acids and *trans*-4-alkoxycinnamic acids as the reason for the formation of liquid crystal phases,^{8,9,10} many reports have used hydrogen bonding in the field of organic liquid crystals.¹¹ In contrast it is surprising, considering the large number of metal-containing liquid crystals (metallomesogens) already known,^{12,13} that only few of them are based on supramolecular species formed by intermolecular hydrogen bonding, namely: a few hydrogen-bonded ferrocene complexes,^{14,15,16} phenanthroline copper derivatives,¹⁷ pyrazole rhodium complexes,¹⁸ and some salicyladimines palladium, copper and vanadium derivatives.¹⁹ This scarcity is probably due to the high melting temperatures often found for metallomesogens, which is hardly compatible with the utilization of moderate or weak hydrogen bonds, as the driving force inducing self-organization above that high melting point.

We have recently reported metallomesogens based on hydrogen bonded supramolecular complexes formed from metalloacids derived from the combination of 4-isocyanobenzoic acid

metal complexes (4-isocyanobenzoic metalloacids, [M]-CNC₆H₄CO₂H), and dodecylstilbazole as proton acceptor.^{20,21} The thermal stability of these dodecylstilbazole aggregates is low and they disaggregate at high temperatures due to the lability of the hydrogen bond. Looking for better thermal stability, we moved to triazines as the hydrogen acceptor, as they make reinforced hydrogen bonds with carboxylic acids.³ This strategy worked for metalloacids derived from iron, chromium, molybdenum and tungsten carbonyls, and afforded columnar mesophases with a peculiar structure consisting of a columnar hexagonal packing of the triazine moieties, with the metal fragments arranged randomly around the columnar interface.²² These hydrogen-bonded columnar systems are interesting because they are soft materials formally similar to a polymer backbone (the column) supporting organometallic fragments, but where both the formation of the column and its connection to the dangling fragments are reversible upon heating or by dissolution. This system permitted to link different metal fragments to the column, thus incorporating properties carried by the metal fragment (color, magnetism, molecular polarizability, electric properties, etc.). New or modified properties might appear in the aggregate arising from the distribution of the metal fragments (e.g. helical structures) or the inter-fragment interactions in the columnar aggregate (e.g. metal-metal interactions along the columnar direction, luminescence from metal-metal bonds, electric monodimensional conductivity along the piled metal fragments). The introduction of fragments of gold (I) in the columnar stacking could be especially interesting because of their ability to establish aurophilic interactions and give functional fluid systems with new properties. However, in previous works we found that the hydrogen bond connection was quite sensitive to the metal forming the 4-isocyanobenzoic metalloacid [M]-CNC₆H₄CO₂H and, to our disappointment, the triazines did not produce aggregates with gold(I) isocyanometalloacids.

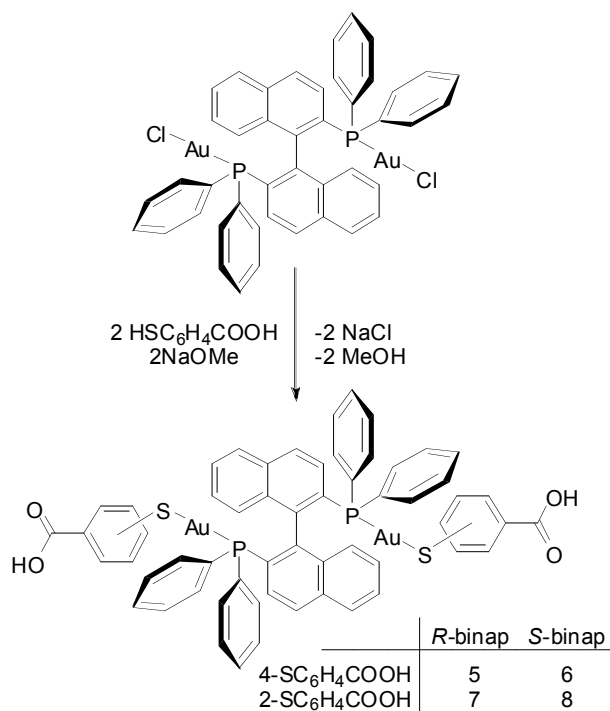
On these grounds, we decided to modify the type of metalloacid, trying to insulate the electronic connection of the metal fragment from the carboxylic acid group, in the hope that this

might induce the formation of a stronger hydrogen bond. Moreover, the use of ligands with different steric requirements might allow for controlling the distribution of the dangling metal fragments along the column and perhaps help for aurophilic interactions. Mono and dinuclear gold thiolate complexes of the type $[\text{Au}(\text{PR}_3)(\text{SC}_6\text{H}_4\text{COOH})]$ and $[\mu\text{-}(\text{binap})\{\text{Au}(\text{SC}_6\text{H}_4\text{COOH})\}_2]$ were chosen as metalloacids to prove the concept. As shown in this paper, these metalloacids react with triazines giving rise to mesomorphic mono and dinuclear hydrogen-bonded triazine-metalloacid aggregates that display stable columnar mesophases at room-temperature. The X-ray studies show that the metal fragments (one per triazine) attached to the triazines by hydrogen bonds act as a wedge between consecutive triazine discogens, which generates a structure with the triazine-metalloacid supramolecules stacked in a complementary manner, in such a way that the steric crowding is minimized and the interface with the aliphatic continuum is smoothed.

Results and Discussion

Synthesis and characterization

The phosphine gold(I) thiolate complexes used as hydrogen donors towards 2,4,6-triarylamino-1,3,5-triazine $[\{(C_{10}H_{21}O)_3C_6H_2NH\}_3C_3N_3]$ (**T**) were $[\text{Au}(\text{PR}_3)(4\text{-SC}_6\text{H}_4\text{COOH})]$ [$R = \text{Cy}$ (**1**), Ph (**2**)],²³ $[\text{Au}(\text{PR}_3)(2\text{-SC}_6\text{H}_4\text{COOH})]$ [$R = \text{Cy}$ (**3**), Ph (**4**)],²⁴ $[\mu\text{-}(\text{P-P})\{\text{Au}(4\text{-SC}_6\text{H}_4\text{COOH})\}_2]$ [$\text{P-P} = R\text{-binap}$ (**5**), $S\text{-binap}$ (**6**)], and $[\mu\text{-}(\text{P-P})\{\text{Au}(2\text{-SC}_6\text{H}_4\text{COOH})\}_2]$ [$\text{P-P} = R\text{-binap}$ (**7**), $S\text{-binap}$ (**8**)]. The binap complexes **5–8** had not been prepared previously, and were synthesized from the corresponding gold chlorophosphine complex, as reported for similar gold derivatives (Scheme 1).²⁴ All phosphine gold(I) thiolate complexes were isolated as air stable white solids. C, H, N analyses, yields, and relevant IR and NMR data for the complexes are given in the experimental part of the Supporting Information.

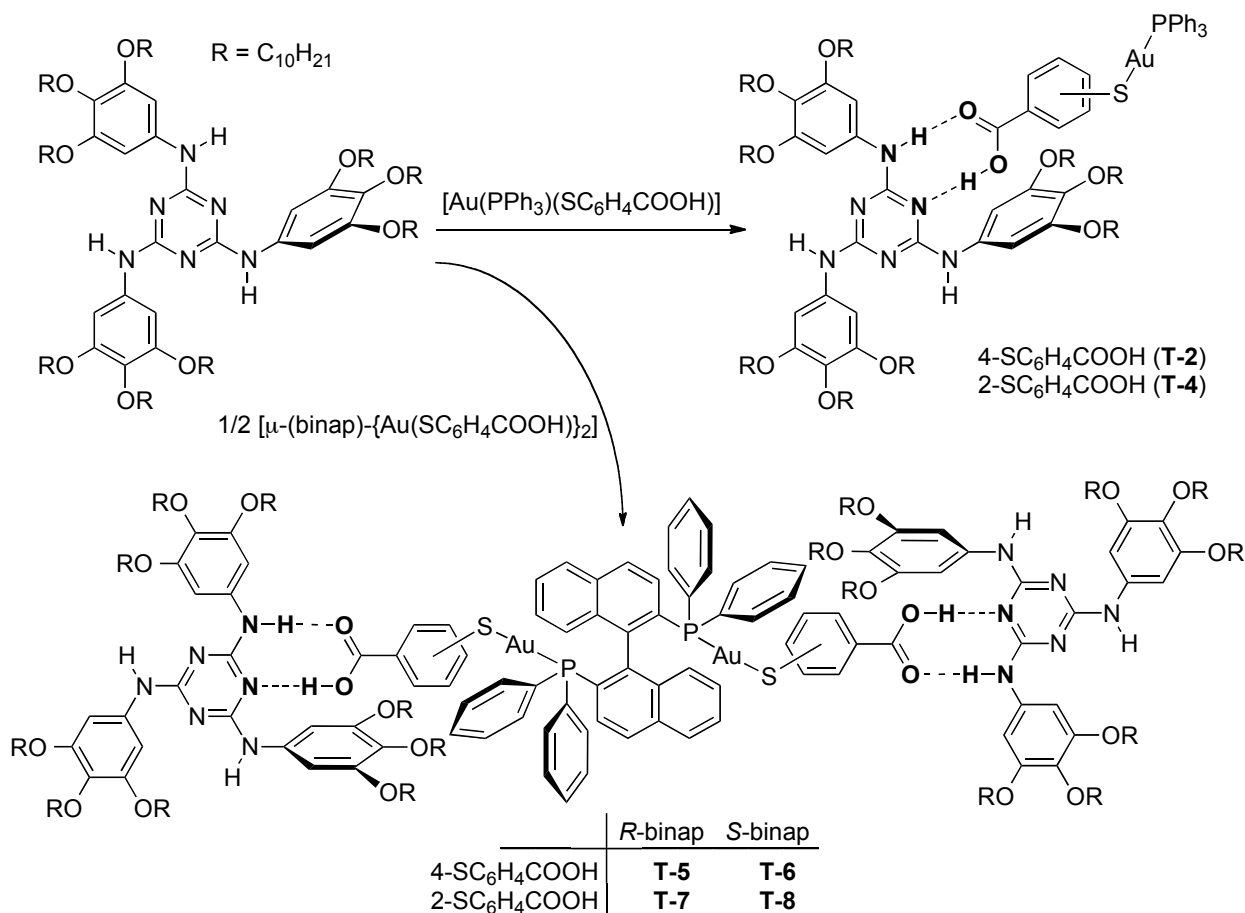


Scheme 1. Synthesis of phosphine gold(I) thiolate complexes

The IR spectra in the solid state of 4-SC₆H₄COOH complexes display one $\nu(\text{C}=\text{O})$ band from the carboxylic group at *ca.* 1675 cm⁻¹ and a broad $\nu(\text{O}-\text{H})$ band in the range 2500-3300 cm⁻¹, consistent with carboxylic acid dimer formation. In contrast, 2-SC₆H₄COOH derivatives show a strong $\nu(\text{C}=\text{O})$ band at *ca.* 1718 cm⁻¹, and three weak bands around 2600, 2645 and 2700 cm⁻¹, which have been assigned to $\nu(\text{OH})$ of carboxylic group involved in an intramolecular O-H...S bond.²⁵ Thus, the derivatives of 2-SC₆H₄COOH acid used in this work have been isolated in a non associated form, which is one of the polymorphs reported for [Au(PCy₃)(2-SC₆H₄COOH)].²⁵ The NMR spectra of the complexes show a singlet signal for ³¹P-¹H, and all the resonances in the ¹H spectra expected for the groups present in the molecule.

Hydrogen-bonded triazine complexes

The hydrogen-bonded triazine-metalloacid complexes were obtained by hydrogen bond interaction of the triazine (**T**) with monocarboxylic and dicarboxylic metalloacids in THF at room-temperature, in 1:1 and 2:1 molar ratios respectively, followed by vacuum evaporation of the solvent, affording the aggregates as pale yellow waxy solids. Note that this means that the various spectroscopic measurements that are made in the absence of solvent correspond to the complex in the mesophase. All the gold metalloacids complexed with aromatic phosphines gave rise to hydrogen-bonded triazine aggregates (labeled as T-metalloacid in **Scheme 2**). This produces changes in the IR spectrum of the aggregates as compared with the starting materials, as discussed below. In contrast, for the gold thiolate complex of tricyclohexylphosphine, the IR spectrum of the gold precursor does not change after treatment with triazine (Table 1), indicating that the desired complexes **T-1** and **T-3** are not formed. In fact, only mixtures of the two unreacted precursors were obtained. The hindrance of the large cone angle PCy₃ ligand (170°) might be the reason for this failure to give aggregation, by precluding the insertion of the metalloacid in the triazine pocket. Thus, only six out of the eight metalloacid complexes used in this work formed supramolecular aggregates with triazine.



Scheme 2. Synthesis of supramolecular triazine-metalloacid gold thiolate complexes. H-bond system in bold.

The IR spectra of these waxy solids in KBr pellets showed the absence of some typical absorptions of the starting components, confirming the formation of the supramolecular complexes in Scheme 2. Thus, they do not show the $\nu(\text{O-H})$ absorptions of the metalloacid phosphine gold thiolate precursors, and the $\nu(\text{C=O})$ band of the carboxylic acid appears clearly shifted from their positions in the parent complexes (Table 1, and Figure S1 in SI). Changes in the $\nu(\text{N-H})$ region are also observed upon formation of the aggregate, as reported for triazine-carboxylic acid aggregates.^{3b} Consequently, the presence of unreacted materials can be discarded, even when assigning the $\nu(\text{O-H})$, $\nu(\text{N-H})$ and $\nu(\text{C=O})$ frequencies for the triazine-metalloacid supramolecular complexes is precluded by the low intensity and large width, for

$\nu(\text{O-H})$ and $\nu(\text{N-H})$ absorptions, or by overlapping of the $\nu(\text{C=O})$ absorptions with the $\nu(\text{C=N})$ triazine bands in the region 1660-1560 cm^{-1} . The weak bands (at 2600, 2645 and 2700 cm^{-1}) associated to intramolecular O-H \cdots S bond, observed in 2- $\text{SC}_6\text{H}_4\text{COOH}$ derivatives, are also lost in the supramolecular triazine aggregates.

Table 1. Selected Infrared spectral data in KBr pellets (cm^{-1}) for the metalloacids and their triazine aggregates.

Compound	Metalloacid $\nu(\text{C=O})$	Triazine aggregate $\nu(\text{C=O})$ or $\nu(\text{C=O}) + \nu(\text{C=N})$
[Au(PCy ₃)(4-SC ₆ H ₄ COOH)] (1)	1674 (s)	1674 (s)
[Au(PPh ₃)(4-SC ₆ H ₄ COOH)] (2)	1675 (s)	1578 (s)
[Au(PCy ₃)(2-SC ₆ H ₄ COOH)] (3)	1719 (s)	1719 (s)
[Au(PPh ₃)(2-SC ₆ H ₄ COOH)] (4)	1718 (s)	1584 (s)
[μ -(<i>R</i> -binap){Au(4-SC ₆ H ₄ COOH)} ₂] (5)	1676 (s)	1585 (s)
[μ -(<i>S</i> -binap){Au(4-SC ₆ H ₄ COOH)} ₂] (6)	1686 (s)	1585 (s)
[μ -(<i>R</i> -binap){Au(2-SC ₆ H ₄ COOH)} ₂] (7)	1719 (s)	1579 (s)
[μ -(<i>S</i> -binap){Au(2-SC ₆ H ₄ COOH)} ₂] (8)	1718 (s)	1583 (s)

The stability of the supramolecular aggregates in solution was investigated by diffusion-ordered NMR spectroscopy (DOSY-NMR; see Figures S2, S3, and S4 in SI), which provides conclusive evidence that metalloacid **5** and triazine (**T**) are dissociated in d^8 -THF, but associated (1:1 ratio) in CDCl_3 . In other words, the stability of the aggregates in solution depends critically on the nature of the interactions with the solvent, and there is no significant dissociation of the aggregate into its components when the aggregate is dissolved in CDCl_3 . The same result is found for aggregate **T-6**. In contrast, for the rest of triazine aggregates in CDCl_3 solution, not all the proton signals exhibit the same diffusion coefficient, revealing that these supramolecular complexes show very significant dissociation of the aggregate into its components. Hence, the supramolecular aggregates derived from 4-sulfanylbenzoic acid are more stable than those derived from 2-sulfanylbenzoic acid, probably because steric hindrance is lower for the former.

Mesomorphic behavior.

The triazine used in this work, $[\{(C_{10}H_{21}O)_3C_6H_2NH\}_3C_3N_3]$, displays a columnar hexagonal mesophase at room-temperature, with a clearing transition at 57 °C.²⁶ In contrast, the metalloacid complexes are not mesomorphic: the 2-thiosalicylic gold complexes melt in the range 157-170 °C, while the 4-thiosalicylic derivatives melt with decomposition above 230 °C. Quite remarkably, all the supramolecular triazine-metalloacid aggregates display enantiotropic liquid crystal behavior at ambient temperature, in temperature ranges quite similar to the parent melamine (Table 2). The mesomorphism of all these gold/melamine supramolecular compounds was studied by polarized optical microscopy (POM), differential scanning calorimetry (DSC), and X-ray scattering. Their optical, thermal and thermodynamic data are collected in Table 2.

Table 2. Optical, thermal and thermodynamic data of triazine-metalloacid aggregates.

Compound	Transition ^a	Temperature ^b (°C)	ΔH^b (kJmol ⁻¹)	ΔS^b (JK ⁻¹ mol ⁻¹)
Melamine (T)	Col _h → I	57	2.0	6.1
T-2	Col _h → I	43	2.3	7.3
T-4	Col _h → I	50	2.6	8.0
T-5	Col _h → I	54	3.2	9.8
T-6	Col _h → I	52	3.3	10.2
T-7	Col _h → I	57	4.8	14.5
T-8	Col _h → I	57	4.7	14.2

^a Col_h, columnar hexagonal; I, isotropic liquid. ^b Data collected from the second heating DSC cycle. The transition temperatures are given as peak onsets.

When viewed with a polarizing microscope on cooling from the isotropic melt, a fluid and homogeneous optical texture displaying pseudo focal conic fan-like optical defects and large black homeotropic regions was observed (Figure 1), which strongly suggests the formation of an uniaxial mesophase. Contact preparations between some complexes and the pure triazine revealed complete mixing, with an approximately linear variation of the isotropization temperature in the mixed zone. No transition lines between both domains were observed, indicating that the mesophases of the supramolecular compounds and the free triazine are equivalent and thus correspond to the same type of packing with the same symmetry. This

mesophase was previously shown to be a columnar phase of hexagonal symmetry (Col_h) in the ligand and is thus kept after the connection of the bulky metalloacid fragments.²² The Col_h phase is also presented by other closely structurally related mesogens with three-fold symmetry.^{3b-c,27}

DSC traces of all the samples were rather silent over all the explored temperature range. Down to low-temperatures (-20°C), still no sign of crystallization or glass transition was detected, but the sample was not as fluid and appeared frozen, suggesting that a glassy state had been reached. The supramolecular complexes have remarkable thermal stability and reach the clearing point with no apparent decomposition. The supramolecular aggregation of triazine with phosphine gold(I) thiolate metalloacids into the supramolecular complexes **T-2** and **T-4** to **T-8**, produces a small decrease in the clearing temperatures and an increase in the clearing enthalpies (consequently an increase of the clearing entropy), compared with the free triazine.

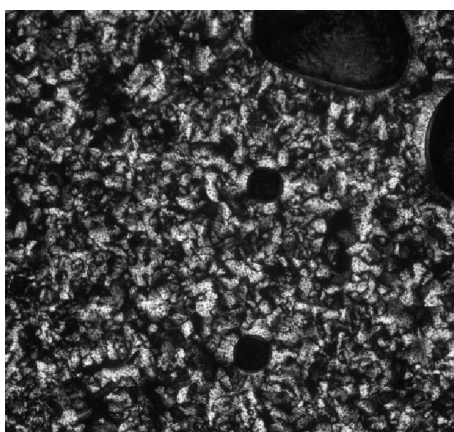


Figure 1. Polarized optical microscopic texture (x 100) observed for **T-7** (chosen as a representative example) on cooling from the isotropic liquid at 45°C .

The mesophase assignment of all six metalloacids-triazine supramolecular complexes (**T-2** and **T-4** to **T-8**) was assessed by powder X-ray diffraction ($2\theta = 0\text{--}30^\circ$) as a function of temperature, from room-temperature up to the isotropic liquid (*ca.* 60°C). In all cases, the diffractograms look similar, confirming that the same type of mesophase is systematically formed for all compounds. They exhibit three characteristics: *i*) One single sharp and intense reflection in the small angle region (Figures 2 and 3), indicative of long-range ordered low-dimensional lattices. *ii*) One broad scattering halo with average maximum located between 8.6

and 10.0 Å (D_i in Table 3). This scattering is not present in the pure triazine patterns and its appearance in the derivatives likely arises from two concomitant causes. First, the column portions containing the gold atoms loom out of the electronic density of the purely organic environment, and thus closest neighbor correlations between these zones should lead to a periodicity lying in this range (see discussion below). Second, a part of the metalloacid fragments protrudes in the low-electronic density aliphatic periphery and likely gives rise to a ribbon of similar periodicity. Consequently, both scatterings would then overlap in the observed diffuse signal. *iii*) A second halo spreading between 3.5 and 5.5 Å (intensity maximum at about 4.3 and 4.4 Å), corresponding to the overlapping of different lateral distances between aliphatic tails and between adduct fragments (h_i in Table 3).

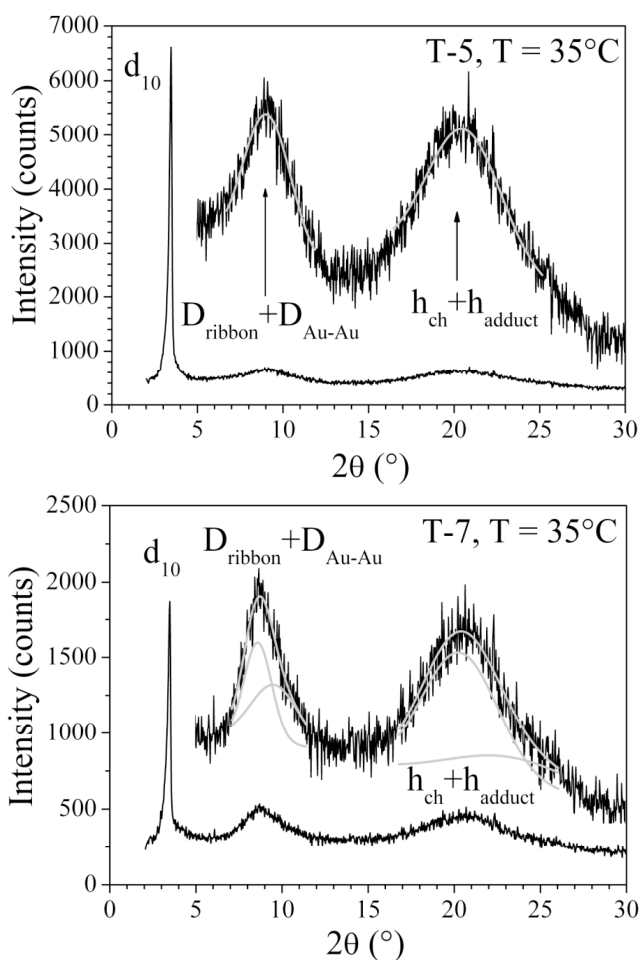


Figure 2. Above: X-ray diffraction patterns for **T-5**. Below: The same for **T-7**. For **T-2** and **T-6** see SI.

The association of these mid-angle broad bands D_i with the metallic fragment is evidenced by the fact that such a scattering is absent in the pure triazine compound itself, and by the substantial angle shift of the maxima observed (Figure 4) with the substitution pattern. For instance, comparing *para*- versus *ortho*-substitution of the peripheral gold fragments, this shift is larger for the latter.

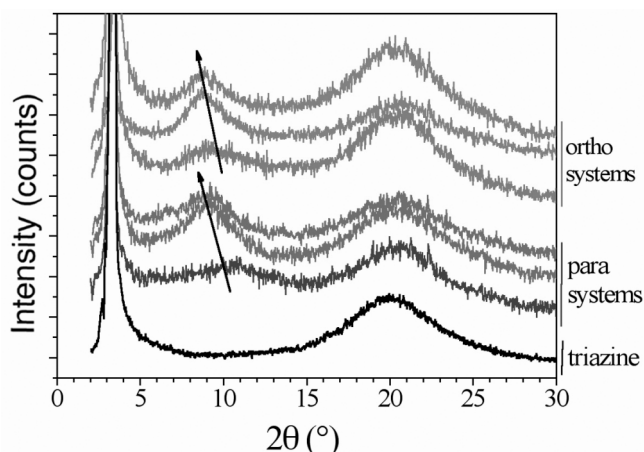


Figure 4: Superimposed XRD patterns of the six triazine-metallo-acid complexes and of the triazine; *para*-isomers **T-2**, **T-5** and **T-6** from bottom to top; *ortho*-isomers **T-3**, **T-7** and **T-8** from bottom to top.

The analysis of these halos suggests that the scatterings of *ortho* derivatives are somewhat dissymmetric (scatterings most generally adopt a symmetric cusp shape, as expected from the widening due to reduced correlation lengths), unlike those of the *para*-compounds (see Figures 2, 4, and S5 and S6 in SI). After elimination of all instrumental sources, this dissymmetry can only be interpreted by the superposition of two halo signals. This conclusion was nicely confirmed by the comparison of the scatterings of monomers and dimers: the global signal shape remains the same, whilst the relative intensity of the overlapping scatterings inverts, resulting in a substantial shift of the apparent scattering maximum. Again, this asymmetry may have several origins, which cannot be clearly discriminated because of the overlapping of scatterings of several zones. Even the ribbon periodicity in the periodicity cannot be excluded as the protruding segments are different for *ortho* and *para* adducts, but intuitively it is more likely related to the

different distribution of gold containing zones. Thus, in the *ortho* adducts, these zones are withdrawn from the column periphery and lead to several overlapping periodicities. The existence of different distances between gold regions has also a molecular explanation, related to the lack of a C_2 rotational axis in the *ortho* fragment of the metalloacid. In the condensed phase the rotation of an *ortho* aryl group must be hindered, which gives rise to, at least, two non-equivalent orientations of this fragment in a disk (atropisomers). The neighboring groups can have coincident or opposite orientations, thus giving rise to different combinations in a column. Not unexpectedly, the *para* derivatives, having a C_2 rotational axis for the thiol fragment cannot produce these atropisomers and give a more symmetric halo. Moreover, since the expected atropisomers of the *ortho* fragments must have different spatial influences above and below the aryl ring, in the supramolecule, this will give rise to planar chirality, which might be interacting with the chirality of the binap systems, defining different diastereomeric supramolecular disks. Furthermore, in the binap systems, helicity of the columns may have been induced by chirality as in other disc-like systems,²⁸ but this possibility could not be evidenced from the diffraction studies.

Table 3. Mesophase parameters.

Compound	T (°C)	d_{10} (Å)	D_i (Å) [ζ (Å)]	h_i (Å) [ζ (Å)]	a (Å)	S(Å ²)
T	30	25.8	-	4.4 [14.6]	29.8	770.4
T-2	30	24.2	8.4 [17.2]	4.3 [19.0]	28.0	677.9
T-4	30	23.3	10.1 [37.5] 8.9 [17.2]	4.4 [14.8] 3.9 [12.2]	26.9	626.9
T-5	35	24.0	9.7 [23.7]	4.3 [15.0]	27.7	665.1
T-6	40	24.1	9.9 [19.7]	4.3 [13.6]	27.8	669.0
T-7	35	23.9	10.2 [41.6] 9.2 [24.3]	4.3 [14.9] 3.8 [9.2]	27.6	660.7
T-8	35	23.9	10.2 [41.6] 9.2 [14.4]	4.4 [24.3] 3.8 [8.1]	27.6	660.7

T: temperature of the X-ray experiment; d_{10} : reflection d_{10} of the hexagonal lattice; D_i and h_i : mid- and large-angle broad scatterings; a: hexagonal lattice parameter; S: cross-columnar section area ($S = a^2\sqrt{3}/2$); D_i : D_{ribbon} , ribbon periodicity (chains and protruding metallo-acid fragments) or/and $D_{\text{Au-Au}}$, first neighbor correlation signal between gold atoms; h_i : h_{ch} , maximum of the diffuse scattering due to lateral distances between molten aliphatic tails, h_{adduct} , diffuse scattering due to lateral distances within columns; ζ : correlation length of the broad signals.

All adducts and the triazine show in their X-ray patterns an intense and sharp first order reflection of the bi-dimensional lattice, and the absence of any higher order reflection. This means that their columns are well confined at the nodes of the long-range correlated lattice (Figure 5), while the interfaces between the high- and low electron density medium (the columns of piled triazine rings and the aliphatic peripheral continuum) are diffuse. For the triazine moiety (Figure 5, above), the link with the molecular architecture is evident: the very symmetrical molecular shape logically leads to equally spaced neighboring columns with an arranged cylindrical shape, leading therefore to an average long-range ordered cylinder packing of $p6mm$ symmetry. However, this highly symmetric long-range organization emerges from a local segregated structure deviating fairly from a regular stacking, as required by the large number of aliphatic tails involved in the mesogen. In fact, the ring volume fraction estimated from reference partial volume data would correspond to cylindrical columns of 13 Å core-diameter, with an envelope area 30% percent smaller than the sum of minimum cross-sections of all molten aliphatic tails (that is 21.4 Å² per completely stretched chain at 30°C, Table 4). Several mechanisms of compensation of the interface area deficiency are known to occur in columnar phases, for instance tilts between stacking direction and columnar axis, possibly associated to a reduced rectangular symmetry, or periodic disruption of columns toward 3-dimensional phases.^{29,30} But here the ring architecture in three branches affords star conformations with large voids at the origin of bumps and hollows in the average cylindrical envelope of columns. With this irregular shape, the envelope area is expanded up to the overall cross-section of tails, but appears as an unsharp interface in X-ray patterns.

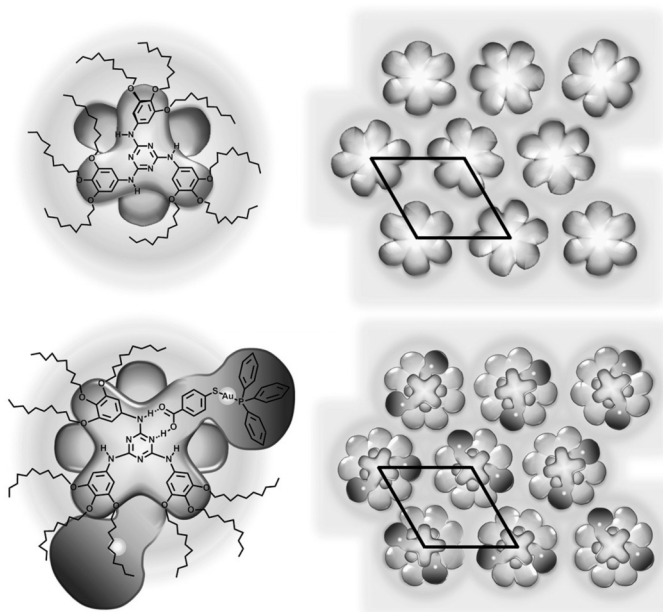


Figure 5. Schematic representations of the two types of long-range ordered $p6mm$ arrangement of cylinders with diffuse interfaces (see text). Above: random alternated stacking in columns and 2D hexagonal lattice of the free triazines. Below: triazine metalloacids associations.

The loose triazine ring architecture allows for intercalation of the different metallo-acid fragments used in this work as a fourth branch of the rings in the supramolecular entity (Figure 5, below). Thus the volume of matter contained inside the average interface cylinder is noticeably increased by formation of the supramolecule and reduces the possibility of surface deformations compensating with tails the lack of interface area. The accordance of areas is then realized by a more classical mechanism consisting in the elongation of columns along the columnar axis, as revealed by the fact that the molecular height per triazine $h_{\text{triaz}} = V_{\text{mol}} / S \cdot N_{\text{triaz}}$ (V_{mol} : molecular volume of the supramolecule; S : columnar cross-section area; N_{triaz} : number of triazines per complex) increases from 3.85 Å in the pure triazine to 5.2-5.6 Å in the corresponding complexes (Table 4). In analogy with macrocycle-type discotic systems for which the macrocycle defines an individual columnar plate,³⁰ these values of h_{triaz} would correspond to columns made of untilted triazine rings with the cores of the associated gold complexes tilted by 45°.

Table 4. Geometrical parameters of mesophases, obtained from XRD.

Compd.	T	V_{mol}	h_{triaz}	$V_{\text{C}}/N_{\text{triaz}}$	$S_{\text{C}}/N_{\text{triaz}}$	$D_{\text{C}}/N_{\text{triaz}}$	a_{ch}	σ_{CH_2}
T	30	2966	3.85	521	135	13.1	17.6	21.39
T-2	30	3518	5.19	686	132	13.0	21.2	21.39
T-3	30	3518	5.61	686	122	12.5	22.0	21.39
T-5	35	7142	5.37	688	128	12.8	21.5	21.47
T-6	40	7164	5.35	690	129	12.8	21.5	21.55
T-7	35	7142	5.41	688	127	12.7	21.6	21.47
T-8	35	7142	5.41	688	127	12.7	21.6	21.47

T is temperature of the experiment in °C; V_{mol} is molecular volume (triazine and adducts) in \AA^3 ; h_{triaz} is molecular height (\AA) per triazine, $h_{\text{triaz}}=V_{\text{mol}}/S_{\text{C}}N_{\text{triaz}}$, where N_{triaz} is the number of triazines per complex ($N_{\text{triaz}} = 1$ for monomers, $N_{\text{triaz}} = 2$ for dimers); V_{C} corresponds to the volume (\AA^3) of the core including that of the triazine part and that of the metallic fragment up the gold atom (e.g. without the phosphine-containing part); S_{C} is the core transverse cross-section area (\AA^2), $S_{\text{C}}=S.V_{\text{C}}/V_{\text{mol}}$; D_{C} is the diameter of the core (\AA), $D_{\text{C}}=2\sqrt{(S_{\text{C}}/\pi)}$; a_{ch} is the area (\AA^2) per fragment on the cylindrical interface, $a_{\text{ch}}=\pi.h.D_{\text{C}}/(n_{\text{ch}}+n_{\text{frag}})$; σ_{CH_2} is the methylene cross-section, $\sigma_{\text{CH}_2}=V_{\text{CH}_2}/1.27$ (\AA^2), where V_{CH_2} (\AA^3)= $26.5616+0.02023T$ (°C).

The statistical area per chain on these elongated average interface cylinders is in perfect agreement with the minimum cross-section of the molten chains, confirming the minor role of the fragment shape irregularities in the architecture adopted by the four branches, (see Table 4; the calculation considers $9+1=10$ chains or emerging segments, and includes the metallo-acid volume fraction bearing the gold-triphenylphosphine segment, which is supposed to protrude from the interface cylinder). Yet, the interface between high and low electron density zones is unsharp in the complexes, as shown by the absence of higher-order reflections in the X-ray pattern, but here the main cause is the high electron density metallo-acid volumes going across the interface defined by the triazine branches. The triphenylphosphine and bi-naphthyl segments lie doubtlessly beyond this interface and interrupt the aliphatic continuum (Figures 2 and 3, D_{ribbon}). The alternation of conjugated and aliphatic parts in these regions might then lead to a ribbon periodicity contributing to the diffuse scattering observed between 8.6 and 10 \AA . Inside the columns, the quite similar molecular segments lead to a quite homogenous electron density, except in the high-density zones containing the gold atoms. First neighbors' correlation between

these zones (Figure 6) would then give rise to an intense scattering, which is presumably the major contribution to the additional diffuse signal (Figures 2 and 3, $D_{\text{Au-Au}}$).

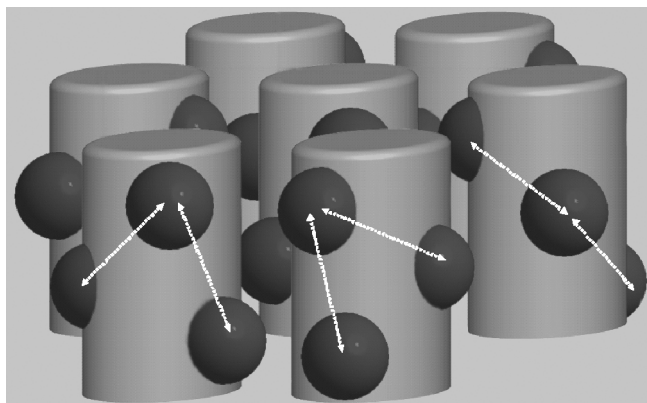


Figure 6. Schematized perspective view of the humped columns packed in hexagonal array, with the white dotted arrows defining either the ribbon periodicity (chains and protruding metalloacid fragments, D_{ribbon}) or/and the first neighbors correlations between gold atoms ($D_{\text{Au-Au}}$).

Unfortunately, the scattering angle is only a rough estimation of the average distance between zones, the effective relation being unknown since it depends on the respective distribution of all interacting first neighbors. This distribution of high electron density regions should be similar for all dimers, as the additional scattering is also very similar. The likely reason for this is the molecular architecture constraining the packing, especially as the structure allows for the location of both triazines in the same column. The only significant difference between *ortho*- and *para*-substituted dimers concerns the dissymmetry of the scattering signal revealing the overlapping of several signals for the former, as discussed above, which is not surprising since their interacting zones should be closer. Conversely, the monomers show weaker and more shifted scatterings.

From the analysis above, idealized representations of the supramolecular arrangements within the Col_h phase can be depicted, both for the pure triazine (**T**) and for the adducts, as shown in Figure 5 for **T-2** chosen as a representative example. It can be seen that the rough interface displayed by the triazine is somehow smoothed upon lateral connection of the “fourth branch” ,

but this fourth branch still protrudes in the aliphatic media because of the bulkiness of the phosphine groups, giving rise to “humped columns” (Figure 6) and to a molecular height increase (Table 4, h_{triaz}). This explains the absence of higher order reflections and the reduced micro segregation with occurrence of ribbons.

Taking into account all our observations, a plausible explanation appears for the clearing temperatures observed for the single triazine molecule as reference, the metallo-pentacarbonyl,²² and the metallo-gold systems. The pentacarbonyl metal fragment is rather small compared to the metallo-phosphines, and is located inside the triazine column. The whole fragment is thus completely embedded within the triazine branches, conferring a more cylindrical shape to the columns, which produces a better segregation as evidenced by the observation of higher order reflections.²² This more efficient packing leads to an increase of the clearing temperature with respect to the free triazine. In contrast, the disturbing effects discussed above for the gold systems are in part compensated by the “fourth branch” filling effect helping to rigidify the columns, which leads to an overall thermal behavior less different from the free triazine.

In summary, uncommon mesomorphic mono and dinuclear hydrogen-bonded triazine-metalloacid aggregates display columnar mesophases at room-temperature with an unusual structure consisting of a columnar stacking of triazine groups and the metal fragments, acting as a wedge of the triazine units and filling the space between the branches of the trifoil molecular architecture. The triazine structure with a high number of lateral chains prove extraordinarily able to “swallow” remarkably large metalorganic fragments attached to it without loosing the mesomorphic behavior. Remarkably, the formation of these supramolecular metalorganic aggregates produces a slight decrease in the clearing temperatures, when compared with the free melamine, probing that this strategy can be very useful for the design of functional materials. The complexes prepared here do not show metallophilic interactions but this strategy looks very

promising for the future design of room-temperature LC mesophases containing interacting metallic fragments.

Experimental Section

Combustion analyses were made with a Perkin-Elmer 2400 microanalyzer. IR spectra (cm^{-1}) were recorded on a Perkin-Elmer FT 1720X instrument and ^1H and ^{19}F NMR spectra on Bruker AC 300 or ARX 300 instruments in CDCl_3 . Microscopy studies were carried out using a Leica DMRB microscope equipped with a Mettler FP82HT hot stage and a Mettler FP90 central processor, at a heating rate of $10\text{ }^\circ\text{C min}^{-1}$. For differential scanning calorimetry (DSC) a Perkin-Elmer DSC7 instrument was used, which was calibrated with water and indium. The scanning rate was $10\text{ }^\circ\text{C min}^{-1}$, the samples were sealed in aluminum capsules in the air, and the holder atmosphere was dry nitrogen. Specific rotations were measured using a Perkin Elmer 343 polarimeter at 589 nm. The XRD patterns were obtained by transmission diffraction with a Guinier experimental set-up. A linear focalized monochromatic $\text{Cu-K}\alpha_1$ beam ($\lambda = 1.5405\text{ \AA}$) was obtained using a sealed-tube generator (900 W) equipped with a bent quartz monochromator. In all cases, the crude powder was filled in thin Lindemann capillaries of 1 mm diameter and $10\text{ }\mu\text{m}$ wall-thickness, in air (corrections for air were made), and then heated to produce the mesophase. An initial set of diffraction patterns was recorded with a curved Inel CPS 120 counter gas-filled detector linked to a data acquisition computer; periodicities up to 70 \AA can be measured, and the sample temperature controlled to within $\pm 0.01\text{ }^\circ\text{C}$ from 20 to $200\text{ }^\circ\text{C}$. Alternatively, patterns were also recorded on an image plate; periodicities up to 120 \AA can be measured (scanned by STORM 820 from Molecular Dynamics with $50\text{ }\mu\text{m}$ resolution). In each case, exposure times were varied from 1 to 24 h.

The gold Complexes $[\text{AuCl}(\text{PCy}_3)]$,³¹ $[(\mu\text{-}S\text{-binap})\text{-(AuCl)}_2]$,³² $[(\mu\text{-}R\text{-binap})\text{-(AuCl)}_2]$,³³ $[\{(\text{C}_{10}\text{H}_{21}\text{O})_3\text{C}_6\text{H}_2\text{NH}\}_3\text{C}_3\text{N}_3]$,^{3b,22} $[\text{Au}(\text{PR}_3)(2\text{-SC}_6\text{H}_4\text{COOH})]$ (R = Cy, Ph),²³ and $[\text{Au}(\text{PPh}_3)(4\text{-SC}_6\text{H}_4\text{COOH})]$ (R = Cy, Ph),^{34,24} had been reported previously and were prepared from a solution of the corresponding chloro complex in dichloromethane, by reaction with the corresponding 2- or 4-sulfanylbenzoic acid (2- or 4-thiosalicylic) acid in methanol with one equivalent amount of sodium methoxide. Preparative procedures and characterization data of the compounds are given in the Supporting Information.

Acknowledgments. This work was sponsored by the Ministerio de Ciencia e Innovación (Project CTQ2011-25137) and the Junta de Castilla y León (Project VA248A11-2). C. D. thanks the Ministerio de Ciencia e Innovación for a studentship. B. D. and B. H. thank the CNRS and the University of Strasbourg for support.

Supporting information. Synthesis and characterization of the compounds; IR spectra (Figure S1); DOSY spectra (Figures S2, S3 and S4); DSC traces; contact experiments; X-ray diffraction patterns (11 pages).

References

- ¹ W. Pisula, M. Kastler, D. Wasserfallen, M. Mondeshki, J. Piris, I. Schnell, K. Müllen, *Chem. Mater.* **2006**, *18*, 3634-3640
- ² a) M. O'Neill, S. M. Kelly, *Adv. Mater.* **2003**, *15*, 1135-1146; b) S. Kumar, *Chem. Soc. Rev.* **2006**, *35*, 83-109; c) S. Laschat, A. Baro, N. Steinke, F. Giesselmann, C. Hägele, G. Scalia, R. Judele, E. Kapatsina, S. Sauer, A. Schreivogel, M. Tosoni, *Angew. Chem. Int. Ed.* **2007**, *46*, 4832-4887; d) S. Sergeyev, W. Pisulab, Y. H. Geerts, *Chem. Soc. Rev.* **2007**, *36*, 1902-1929.
- ³ a) D. Goldmann, R. Dietel, D. Janietz, C. Schmidt, J. H. Wendorff, *Liq. Cryst.* **1998**, *24*, 407-411; b) J. Barberá, L. Puig, J. L. Serrano, T. Sierra, *Chem. Mater.* **2004**, *16*, 3308-3317; c) J. Barberá, L. Puig, J. L. Serrano, T. Sierra, *Chem. Mater.* **2005**, *17*, 3763-3771.
- ⁴ a) S. Coco, P. Espinet, J.-M. Martín-Alvarez, A. M. Levelut, *J. Mater. Chem.* **1997**, *7*, 19-23; b) J. Barberá, A. Elduque, R. Giménez, F. J. Lahoz, J. A. Lopez, L. A. Oro, J. L. Serrano, *Inorg. Chem.* **1998**, *37*, 2960-2967; c) S. J. Kim, S. H. Kang, K.-M. Park, H. Kim, W.-C. Zin, M.-G. Choi, K. Kim, *Chem. Mater.* **1998**, *10*, 1889-1893; d) M. Benouazzane, S. Coco, P. Espinet, J.-M. Martín-Alvarez, *J. Mater. Chem.* **1999**, *9*, 2327-2332; e) M. Benouazzane, S. Coco, P. Espinet, J.-M. Martín-Alvarez, J. Barberá, *J. Mater. Chem.* **2002**, *12*, 691-696; f) C. Cordovilla, S. Coco, P. Espinet, B. Donnio, *J. Am. Chem. Soc.* **2010**, *132*, 1424-1431; g) R. Perochon, P. Davidson, S. Rouzière, F. Camerel, L. Piekara-Sady, T. Guizouarn, M. Fourmigué, *J. Mater. Chem.* **2011**, *21*, 1416-1422.

⁵ M. Suárez, J.-L. Lehn, S. C. Zimmerman, A. Skoulios, B. Heinrich, *J. Am. Chem. Soc.* **1998**, *120*, 9526-9532.

⁶ J. Kang, J. Santamaría, G. Hilmersson, J. Rebek, *J. Am. Chem. Soc.* **1998**, *120*, 7389-7390.

⁷ V. Balzani, A. Credi, F. M. Raymo, J. F. Stoddart, *Angew. Chem., Int. Ed.* **2000**, *39*, 3348-3391.

⁸ G. W. Gray, in *Molecular Structure and Liquid Crystals*, Academic Press: London, **1967**, p. 161, and references therein.

⁹ *Handbook of Liquid Crystals*, (Eds.: D. Demus, J. Goodby, G. W. Gray, H. W. Spiess, D. V. Vill), Wiley-VCH: Weinheim, **1998**.

¹⁰ a) A. E. Bradfield, B. J. Jones, *J. Chem. Soc.* **1929**, 2660-2661; b) G. W. Gray, B. Jones, *J. Chem. Soc.* **1953**, 4179-4180.

¹¹ a) T. Kato, J. M. Fréchet, *J. Am. Chem. Soc.* **1989**, *111*, 8533-8534; b) M.-J. Brienne, J. Gabard, J.-M. Lehn, I. Stibor, *J. Chem. Soc. Chem. Commun.* **1989**, 1868-1870; c) K. Willis, D. J. Price, H. Adams, G. Ungar, D. W. Bruce, *J. Mater. Chem.* **1995**, *5*, 2195-2199; d) C. Tschierske, *Prog. Polym. Sci.* **1996**, *21*, 775-852; e) C. M. Paleos, D. Tsiourvas, *Liq. Cryst.* **2001**, *28*, 1127-1161; f) D. W. Bruce, *Advances in Inorganic Chemistry* **2001**, *52*, 151-204; g) M. Grunet, R. A. Howie, A. Kaeding, C. T. Imrie, *J. Mater. Chem.* **1997**, *7*, 211-214; h) F. Würthner, S. Yao, B. Heise, C. Tschierske, *Chem. Commun.* **2001**, *14*, 2260-2261; i) N. Mizoshita, H. Monobe, M. Inoue, M. Ukon, T. Watanabe, Y. Shimizu, K. Hanabusa, T. Kato, *Chem. Commun.* **2002**, 428-429; j) S. Jin, Y. Ma, S. C. Zimmerman, S. Z. D. Cheng, *Chem. Mater.* **2004**, *16*, 2975-2977; k) T. Kajitana, S. Kohmoto, M. Yamamoto, K. Kishikawa, *Chem. Mater.* **2004**, *16*, 2329-2331; l) J. A. McCubbin, X. Tong, Y. Zhao, V. Snieckus, R. P. Lemieux, *Chem. Mater.* **2005**, *17*, 2574-2581; m) J. Barberá, L. Puig, P. Romero, J. L. Serrano, T. Sierra, *J. Am. Chem. Soc.* **2006**, *128*, 4487-4492; n) T. Kato, N. Mizoshita, K. Kishimoto, *Angew. Chem. Int. Ed.* **2006**, *45*, 38-68.

¹² a) P. Espinet, M. A. Esteruelas, L. Oro, J. L. Serrano, E. Sola, *Coord. Chem. Rev.* **1992**, *117*, 215-274; b) *Metallomesogens* (Ed.: J. L. Serrano), VCH: Weinheim, **1996**; c) B. Donnio, D. Guillon, D. W. Bruce, R. Deschenaux, in *Metallomesogens, Comprehensive Organometallic Chemistry III: From Fundamentals to Applications*, Vol. 12, (Eds.: R. H. Crabtree, D. M. P. Mingos), Elsevier: Oxford, UK, **2006: Applications III: Functional Materials, Environmental and Biological Applications, (Ed.: D. O'Hare), ch. 12.05, pp. 195-294.**

¹³ D. W. Bruce, in *Inorganic Materials* (Eds.: D. W. Bruce, D. O'Hare), Wiley: Chichester, 2nd edition, **1996**, ch. 8.

¹⁴ R. Deschenaux, F. Monnet, E. Serrano, F. Turpin, A.-M. Levelut, *Helv. Chim. Acta* **1998**, *81*, 2072-2077.

¹⁵ P. Massiot, M. Imperor-Clerc, M. Veber, R. Deschenaux, *Chem. Mater.* **2005**, *17*, 1946-1951.

¹⁶ B. Donnio, J. M. Seddon, R. Deschenaux, *Organometallics* **2000**, *19*, 3077-3081.

¹⁷ R. Ziessel, G. Pickaert, F. Camerel, B. Donnio, D. Guillon, M. Cesario, T. Prangé, *J. Am. Chem. Soc.* **2004**, *126*, 12403-12413.

¹⁸ R. Giménez, A. Elduque, J. A. López, J. Barberá, E. Cavero, I. Lantero, L. A. Oro, J. L. Serrano, *Inorg. Chem.* **2006**, *45*, 10363-10370

¹⁹ a) S.-Y. Li, C.-J. Chen, P.-Y. Lo, H.-S. Sheu, G.-H. Lee, C. K. Lai, *Tetrahedron* **2010**, *66*, 6101-6112; b) Y. J. Wang, J. H. Song, Y. S. Lin, C. Lin, H. S. Sheu, G. H. Lee, C. K. Lai, *Chem. Commun.* **2006**, 4912-4914

²⁰ S. Coco, E. Espinet, P. Espinet, I. Palape, *Dalton Trans.* **2007**, 3267-3272.

²¹ S. Coco, C. Cordovilla, C. Domínguez, P. Espinet, *Dalton Trans.* **2008**, 6894-6900.

²² S. Coco, C. Cordovilla, C. Domínguez, B. Donnio, P. Espinet, D. Guillon, *Chem. Mater.*

2009, *21*, 3282–3289.

²³ D. De Vos, P. Clements, S. M. Pyke, D. R. Smyth, E. R. T. Tiekink, *Metal-Based Drugs* **1999**, *6*, 31-40.

²⁴ J. D. E. T. Wilton-Ely, A. Schier, N. Mitzel, H. Schmibaur, *J. Chem. Soc. Dalton. Trans.* **2001**, 1058-1062.

²⁵ D. R. Smyth, B. R. Vincent, E. R. T. Tiekink, *Crystal Growth & Design.* **2001**, *1*, 113-117

²⁶ This triazine has been reported in ref. 3b. However, there is a significant discrepancy between the reported clearing temperature and that measured in this work.

²⁷ a) D. J. Pesak, J. S. Moore, *Angew. Chem. Int. Ed. Engl.* **1997**, *36*, 1636-1639; b) H. Meier, M. Lehmann, *Angew. Chem. Int. Ed. Engl.* **1998**, *37*, 643-645; c) A. Omenat, J. Barberá, J. L. Serrano, S. Houbrechts, A. Persoons, *Adv. Mater.* **1999**, *11*, 1292-1295; d) H. Meier, M. Lehmann, U. Kolb, *Chem. Eur. J.* **2000**, *6*, 2462-2469; e) C. H. Lee, T. Yamamoto, *Tetrahedron Lett.* **2001**, *42*, 3993-3996; f) A.-J. Attias, C. Cavalli, B. Donnio, D. Guillon, P. Hapiot, J. Malthête, *Chem. Mater.* **2002**, *14*, 375-384; g) H. Meier, H. C. Holst, A. Oehlhof, *Eur. J. Org. Chem.* **2003**, 4173-4180; h) M. Lehmann, M. Jahr, B. Donnio, R. Graf, S. Gemming, I. Popov, *Chem. Eur. J.* **2008**, *14*, 3562-3576.

²⁸ J. Grolik, L. Dudek, J. Eilmes, A. Eilmes, M. Gorecki, J. Frelek, B. Heinrich, B. Donnio, *Tetrahedron* **2012**, *68*, 3875-3884, and references therein.

²⁹ I. Bury, B. Heinrich, C. Bourgoigne, G. H. Mehl, D. Guillon, B. Donnio, *New J. Chem.* **2012**, *36*, 452–468.

³⁰ D. Myśliwiec, B. Donnio, P. J. Chmielewski, B. Heinrich, M. Stepień, *J. Am. Chem. Soc.* **2012**, *134*, 4822-4833.

³¹ R. C. Bott, G. A. Bowmaker, R. W. Buckley, P. C. Healy, M. C. S. Perera, *Aust. J. Chem.* **1999**, *52*, 271-277.

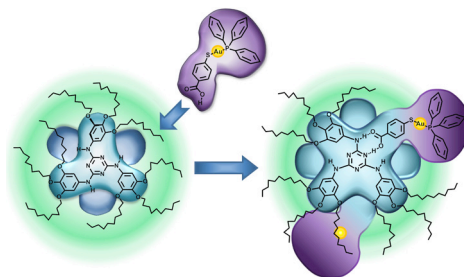
³² C. A. Wheaton, M. C. Jennings, R. J. Puddephatt, *Z. Naturforsch.* **2009**, *64b*, 1469-1477.

³³ M. P. Muñoz, J. Adrio, J. C. Carretero, A. M. Echavarren, *Organometallics* **2005**, *24*, 1293-1300.

³⁴ D. De Vos, D. R. Smyth, E. R. T. Tiekink, *Metal-Based Drugs* **2002**, *8*, 303-306.

Table of Contents Graphic

Mono and dinuclear hydrogen-bonded triazine-thiolategold(I)metalloacid aggregates display stable columnar mesophases at room-temperature with the metal fragments acting as a wedge between the columnar stacking of triazine discogens.



Supporting Information to:

Room Temperature Columnar Mesophases in Triazine/Gold-Thiolate Metalorganic Supramolecular Aggregates

*Cristina Domínguez,^a Benoît Heinrich,^b Bertrand Donnio,^b Silverio Coco,^{*a} and Pablo Espinet.^{*a}*

^a IU CINQUIMA/Química Inorgánica, Facultad de Ciencias, Universidad de Valladolid, 47071 Valladolid, Castilla y León, Spain. ^b Institut de Physique et Chimie des Matériaux de Strasbourg (IPCMS), UMR 7504 (CNRS-ULP), 23 rue du Loess, BP 43, F-67034 Strasbourg Cedex 2 (France).

1.- SYNTHESIS AND CHARACTERIZATION OF THE COMPOUNDS

Preparation of [(μ -*R*-binap){Au(4-SC₆H₄COOH)}₂] (5). A solution of [4-HSC₆H₄COOH] (17.54 mg, 0.11 mmol) and sodium methoxide (6.73 mg, 0.12 mmol) in methanol (5 mL) was added dropwise to a stirred solution of [(μ -*R*-binap)-(AuCl)₂] (60.00 mg, 0.06 mmol) in dichloromethane (15 mL). After stirring for 90 min. at room temperature, the solvent was removed under vacuum. The resulting residue was extracted in dichloromethane. Hexane was added to precipitate the product as a white solid (0.06 g, 81 % yield). M.p.(dec) = 236 °C. IR (KBr/cm⁻¹): ν (C=O): 1675 (s). [α]²⁰ = +77 (c = 0.35, THF). ¹H NMR (CDCl₃): δ 12.80 (s, br, 1H, COOH), 8.10 (d, *J* = 8.49 Hz, 2H), 7.81 (m, 6H), 7.67 (m, 6H), 7.49 (m, 4H), 7.42 (m, 2H), 7.33 (m, 2H), 7.25-6.99 (m, 11H), 6.49-6.30 (m, 4H). ³¹P {¹H} NMR (CDCl₃): d 33.15 (s). Anal. Calcd. for C₅₈H₄₂Au₂O₄P₂S₂: C, 52.66; H, 3.20. Found: C, 52.50; H, 3.02.

Preparation of [(μ -*S*-binap)-{Au(4-SC₆H₄COOH)}₂] (6). This compound was prepared as for [(μ -*R*-binap)-{Au(4-SC₆H₄COOH)}₂], starting from [(μ -*R*-binap)-(AuCl)₂] (60.00 mg, 0.06 mmol). The product was isolated as a white solid. (0.06 g, 81 % yield). m.p.(dec) = 237 °C. IR (KBr/cm⁻¹): μ (C=O): 1686 (s). [α]²⁰ = -77 (c = 0.25, THF). ¹H NMR (CDCl₃): δ 12.80 (s, br, 1H, COOH), 8.09 (d, *J* = 8.88 Hz, 2H),

7.81 (m, 6H), 7.66 (m, 6H), 7.49 (m, 4H), 7.41 (m, 2H), 7.33 (m, 2H), 7.25-7.1 (m, 11H), 6.49-6.30 (m, 4H). ^{31}P $\{^1\text{H}\}$ NMR (CDCl_3): d 33.16 (s). Anal. Calcd. for $\text{C}_{58}\text{H}_{42}\text{Au}_2\text{O}_4\text{P}_2\text{S}_2$: C, 52.66; H, 3.20. Found: C, 52.55; H, 3.12.

Preparation of $[(\mu\text{-}R\text{-binap})\text{-}\{\text{Au}(2\text{-SC}_6\text{H}_4\text{COOH})\}_2]$ (7). This compound was prepared as for $[(\mu\text{-}R\text{-binap})\{\text{Au}(4\text{-SC}_6\text{H}_4\text{COOH})\}_2]$, starting from [2-HSC₆H₄COOH] (17.54 mg, 0.11 mmol), sodium methoxide (6.73 mg, 0.12 mmol) and $[(\mu\text{-}S\text{-binap})(\text{AuCl})_2]$ (60.00 mg, 0.06 mmol). The product was isolated as a white solid. (0.05 g, 69 % yield). m.p. = 157 °C. IR (KBr/cm⁻¹): $\mu(\text{C}=\text{O})$: 1719 (s). $[\alpha]^{20} = -11$ (c = 0.5, THF). ^1H NMR (CDCl_3): δ 12.99 (s, br, 1H, COOH), 8.30 (dd, $J_1 = 7.61$ Hz, $J_2 = 1.81$ Hz, 2H), 8.04 (d, $J = 8.60$ Hz, 2H), 7.83 (d, $J = 8.14$ Hz, 2H), 7.53-7.40 (m, 17H), 7.38-6.98 (m, 17H), 6.73 (m, 2H). ^{31}P $\{^1\text{H}\}$ NMR (CDCl_3): d 28.83 (s). Anal. Calcd. for $\text{C}_{58}\text{H}_{42}\text{Au}_2\text{O}_4\text{P}_2\text{S}_2$: C, 52.66; H, 3.20. Found: C, 52.56; H, 3.05.

Preparation of $[(\mu\text{-}S\text{-binap})\text{-}\{\text{Au}(2\text{-SC}_6\text{H}_4\text{COOH})\}_2]$ (8). This compound was prepared as for $[(\mu\text{-}S\text{-binap})\text{-}\{\text{Au}(4\text{-SC}_6\text{H}_4\text{COOH})\}_2]$, starting from [2-HSC₆H₄COOH] (17.54 mg, 0.11 mmol), sodium methoxide (6.73 mg, 0.12 mmol) and $[(\mu\text{-}S\text{-binap})(\text{AuCl})_2]$ (60.00 mg, 0.06 mmol). The product was isolated as a white solid. (0.07 g, 96 % yield). m.p. = 158 °C. IR (KBr/cm⁻¹): $\mu(\text{C}=\text{O})$: 1718 (s). $[\alpha]^{20} = +11$ (c = 0.3, THF). ^1H NMR (CDCl_3): δ 12.99 (s, br, 1H, COOH), 8.31 (dd, $J_1 = 7.56$ Hz, $J_2 = 1.67$ Hz, 2H), 8.04 (d, $J = 8.59$ Hz, 2H), 7.83 (d, $J = 8.14$ Hz, 2H), 7.55-6.95 (m, 34H), 6.73 (d, 2H). ^{31}P $\{^1\text{H}\}$ NMR (CDCl_3): δ 28.91 (s). Anal. Calcd. for $\text{C}_{58}\text{H}_{42}\text{Au}_2\text{O}_4\text{P}_2\text{S}_2$: C, 52.66; H, 3.20. Found: C, 52.96; H, 3.50.

Preparation of hydrogen-bonded triazine complexes. The supramolecular complexes were prepared from the pure components. Exact stoichiometric molar amounts of the two compounds were dissolved in dry tetrahydrofuran at room temperature, and the solvent was pumped off in vacuum, affording the aggregates as pale yellow waxy solids.

The supramolecular triazine-metalloacid aggregates containig binap ligands, maintain the chiral character of their gold precursors. Their specific rotation measurements ($[\alpha]^{20}$) in CH_2Cl_2 solution are: -20° (**T-5**), $+20^\circ$ (**T-6**), $+2^\circ$ (**T-7**), -2° (**T-8**).

2.- EXAMPLE OF FTIR CHARACTERIZATION OF TRIAZINE AGGREGATES

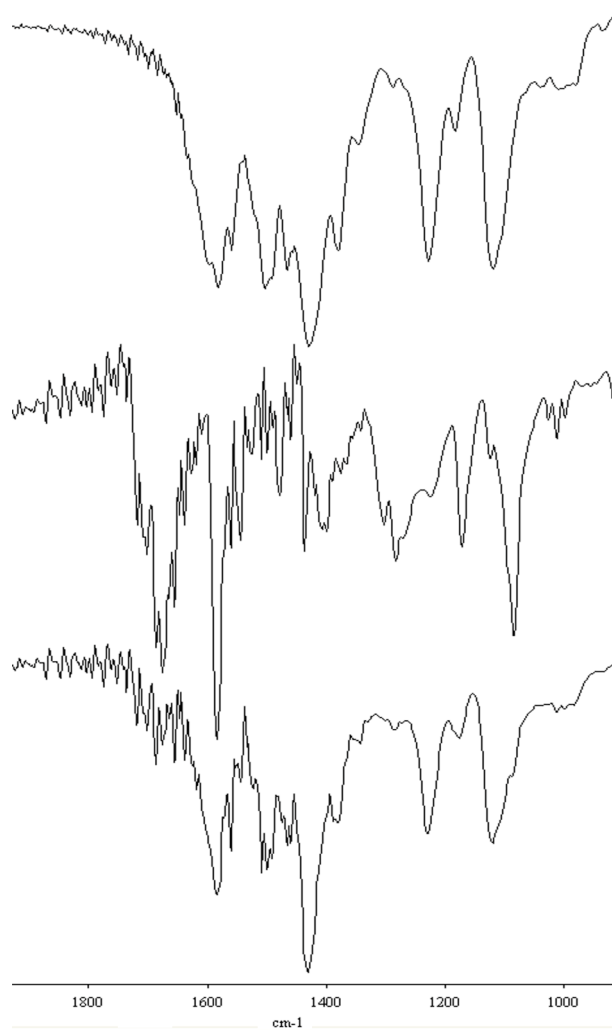


Figure S1. FTIR spectra of free triazine (up), metalloacid (**5**) (middle) and its triazine aggregate (**T-5**) (down).

3.- DOSY SPECTROSCOPIC STUDIES.

This technique allows correlating the diffusion coefficients of solute molecules of different sizes. It has been successfully applied to study molecular association in different complex systems, including H-bonded complexes and supramolecular liquid crystals.^{1,2} The DOSY studies were performed in THF and in CDCl₃ solutions.

The two-dimensional spectra shown in Figures S2 and S3 represent chemical shifts against diffusion coefficients (logarithmic scale) for the supramolecular complex **T-5**. The spectra show that signals corresponding the two components of the aggregate show different diffusion coefficients in d⁸-THF, whereas to all these protons exhibit the same diffusion coefficient in CDCl₃. These results provide conclusive evidence that metalloacid **5** and triazine (**T**) are associated in a 1:1 ratio, making a discrete supramolecule (**T-5**) that is stable in CDCl₃. The same results are found for aggregate **T-6**.

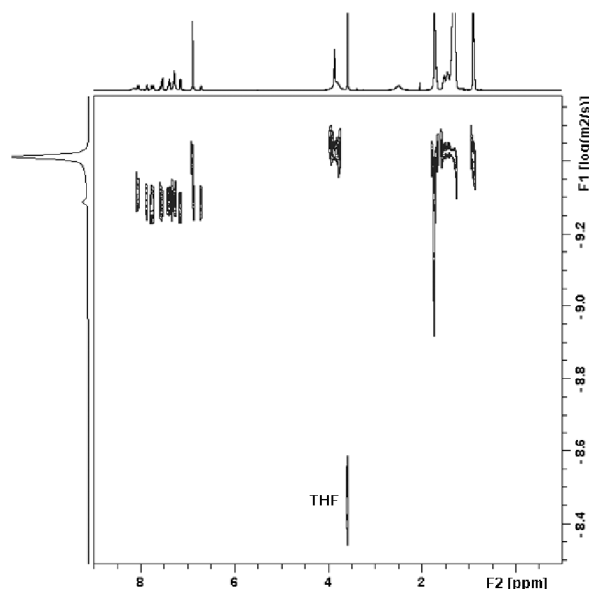


Figure S2. DOSY spectra of complex (**T-5**) in d⁸-THF. Note that the two resonances of THF appear with apparent different diffusion coefficients. This effect is due to some overlapping of resonances of triazine and high field signal of THF.

¹ Barberá, J.; Puig, L.; Serrano, J. L.; Sierra, T. *Chem. Mater.* **2005**, *17*, 3763-3771.

² Cohen, Y.; Avram, L.; Frish, L. *Angew. Chem., Int. Ed.* **2005**, *44*, 520-554.

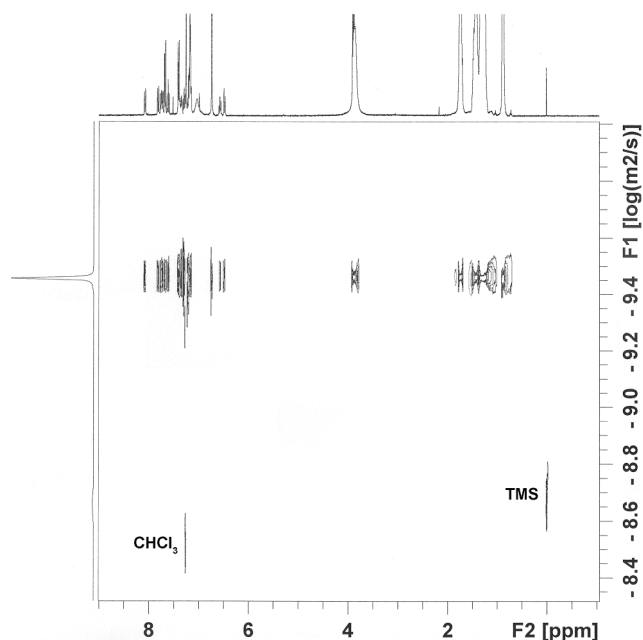


Figure S3. DOSY spectra of complex (**T-5**) in CDCl_3 .

In contrast, for the rest of triazine aggregates (e.g. **T-7**, Figure S4), not all the protons signals exhibit the same diffusion coefficient, revealing that these supramolecular complexes are not stable in CDCl_3 solution, and the triazine and the metalloacid behave as independent components. Hence, the supramolecular aggregates derived from 4-sulfanylbenzoic acid are more stable than those derived from 2-sulfanylbenzoic acid, probably because the former are less crowded.

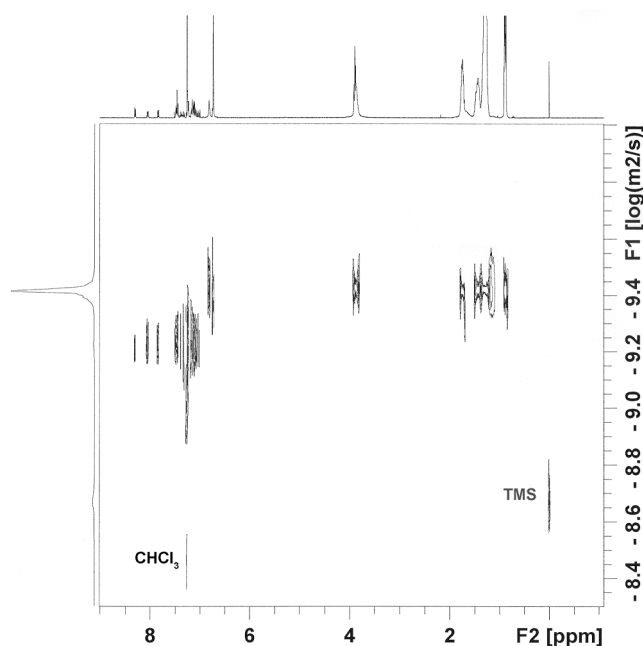
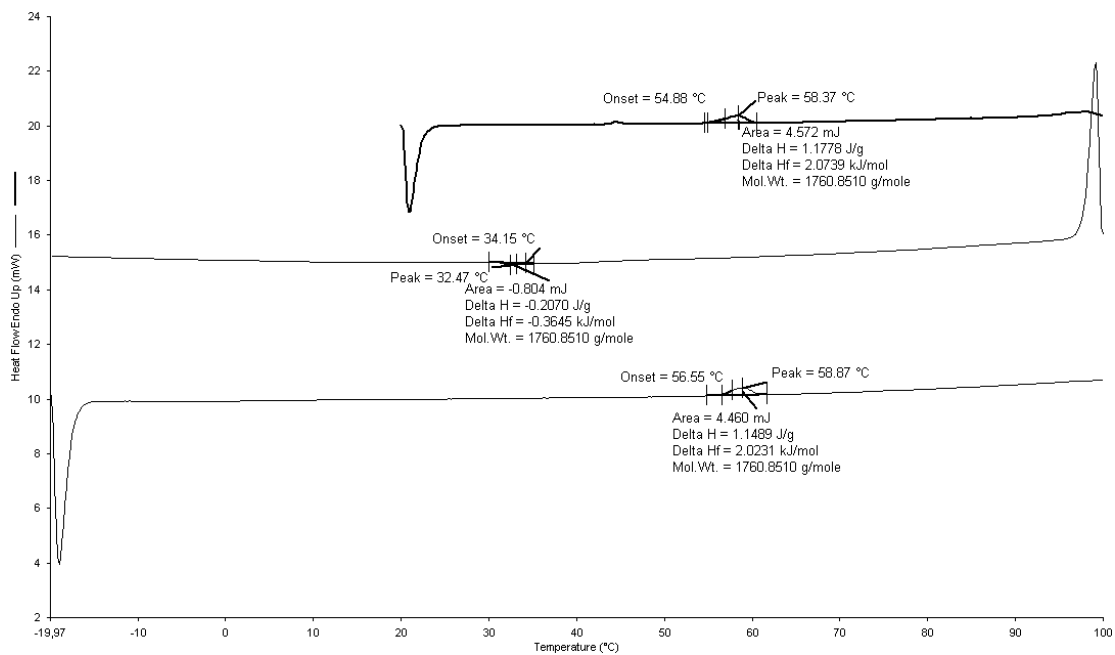


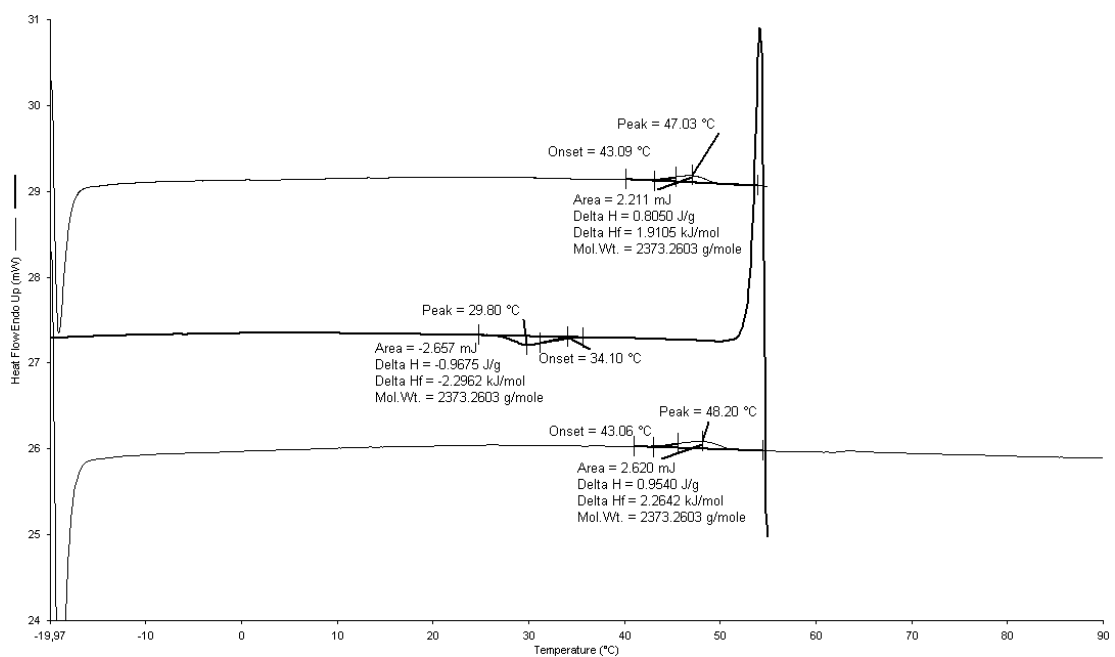
Figure S4. DOSY spectra of complex (**T-7**) in CDCl_3 .

4. DSC thermograms (first heating (up), cooling (middle), second heating (down)).

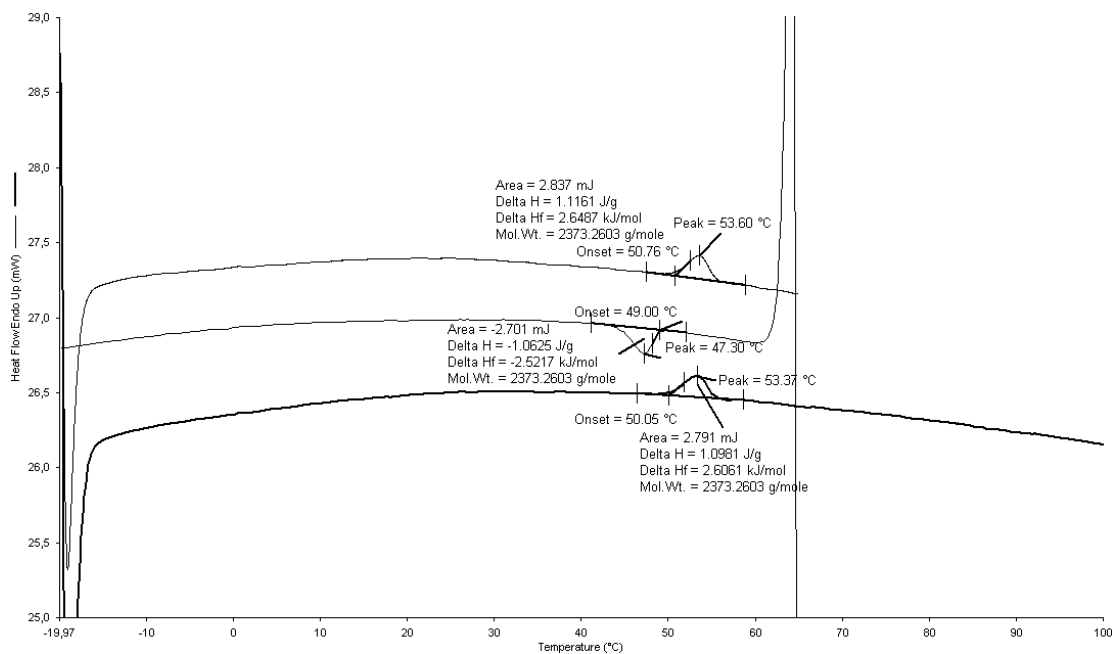
Free triazine



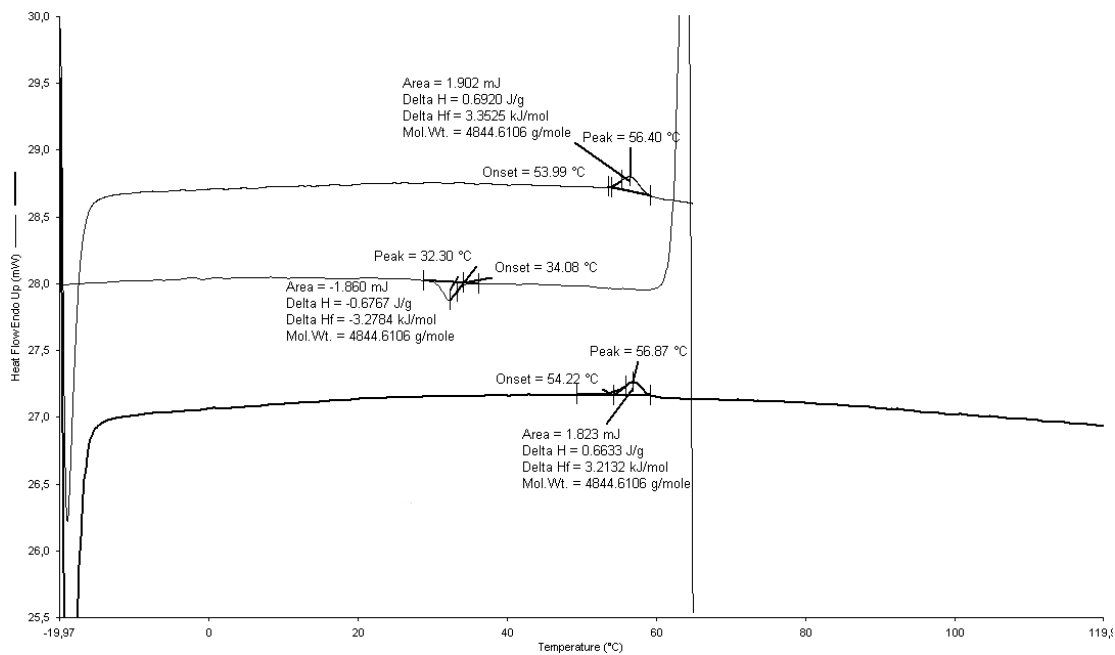
T-2 aggregate



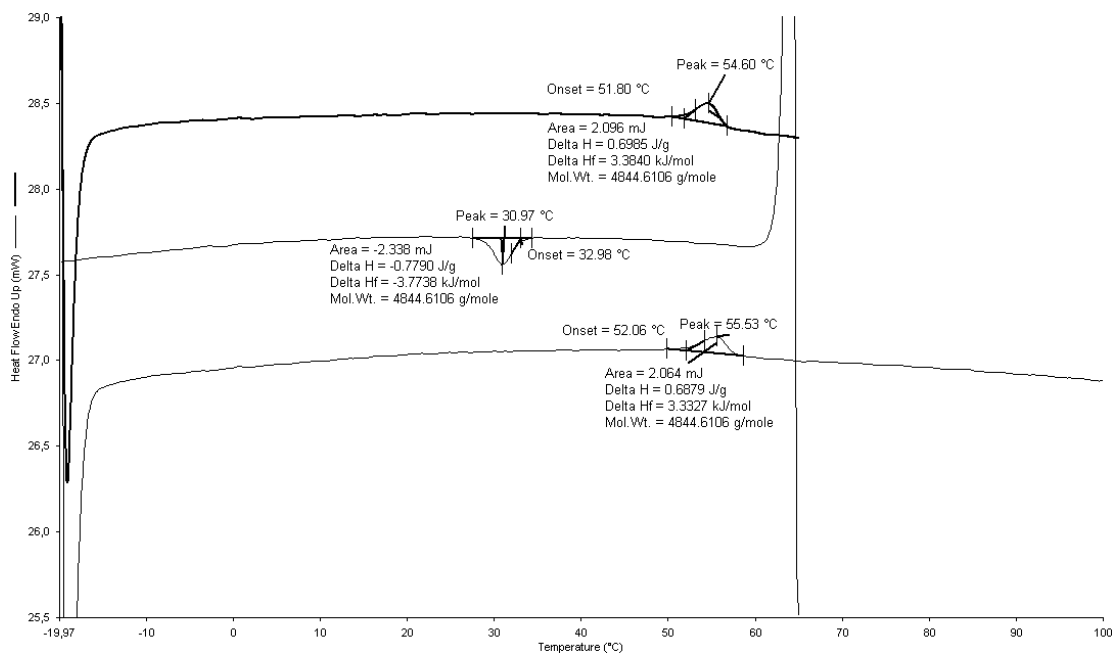
T-4 aggregate



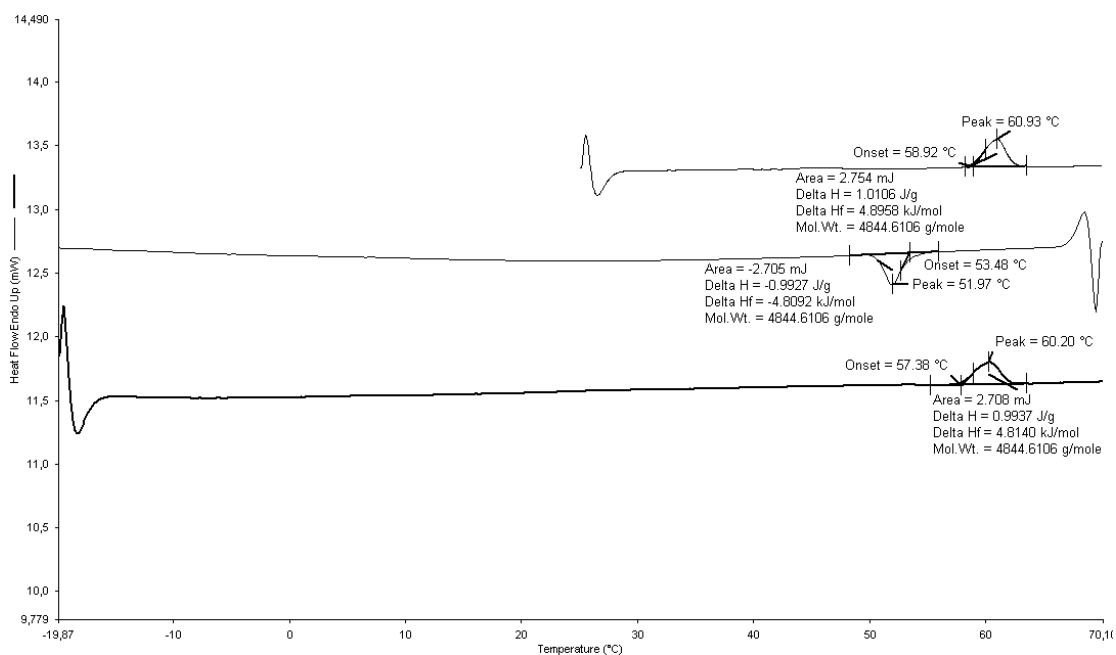
T-5 aggregate



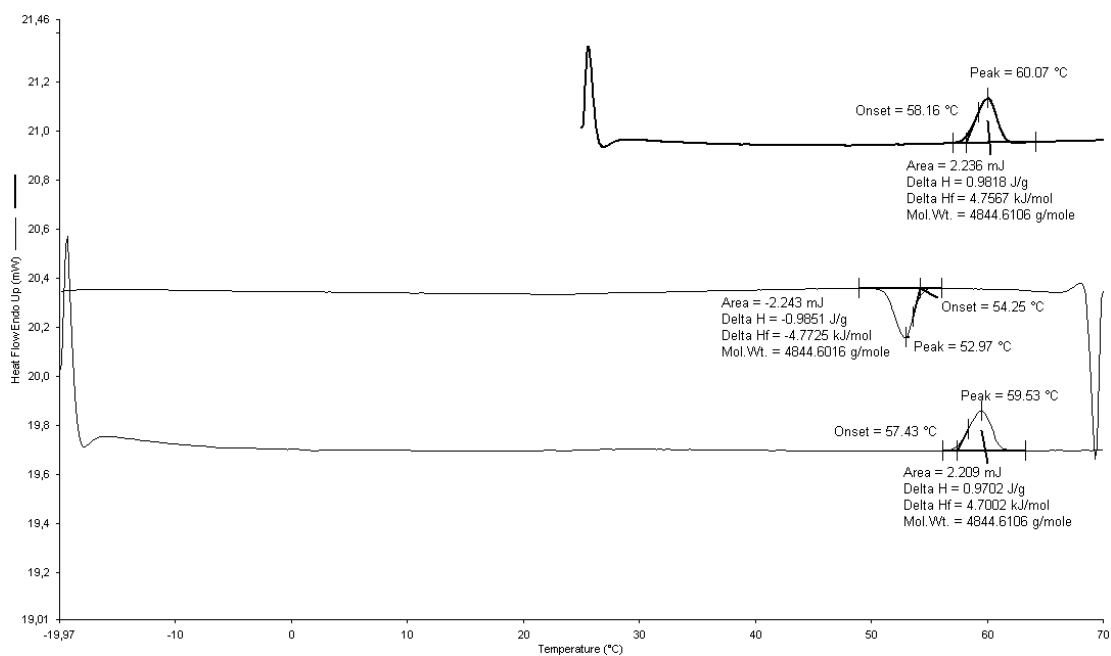
T-6 aggregate



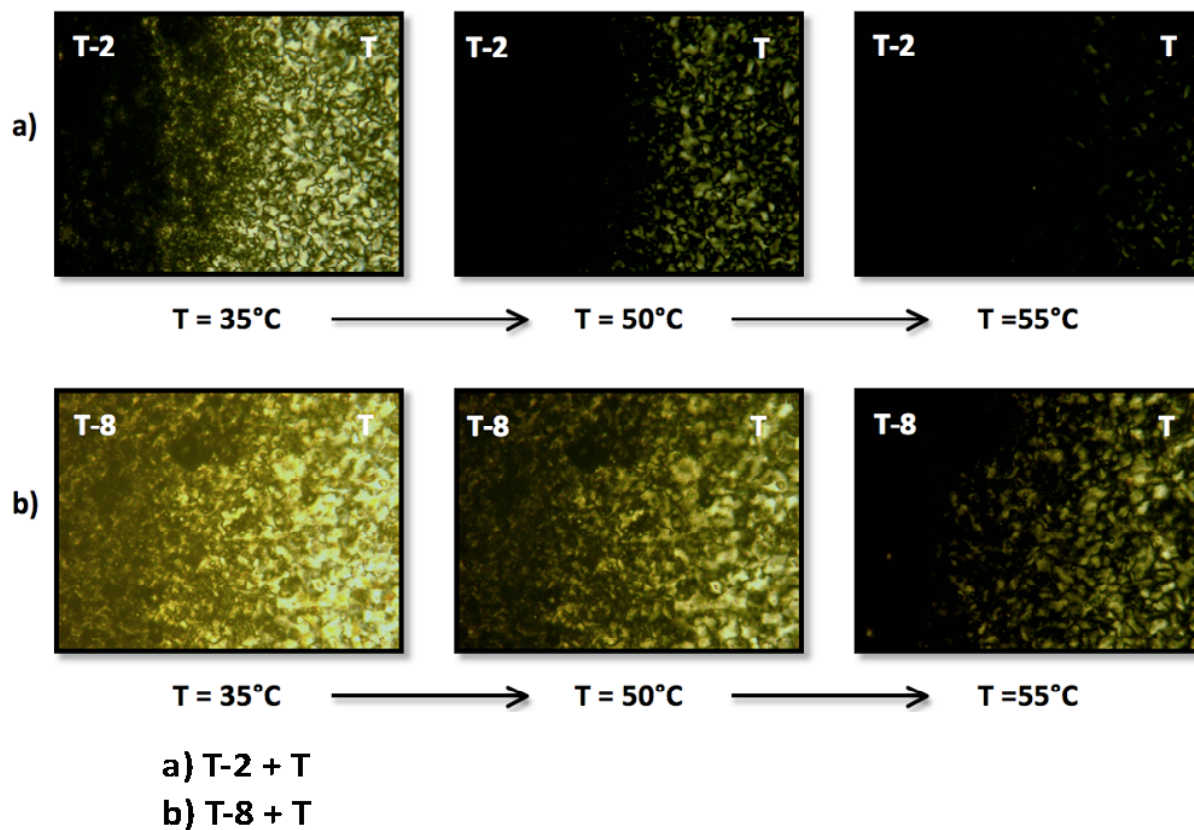
T-7 aggregate



T-8 aggregate



5. Contact preparations between some complexes and the pure triazine.



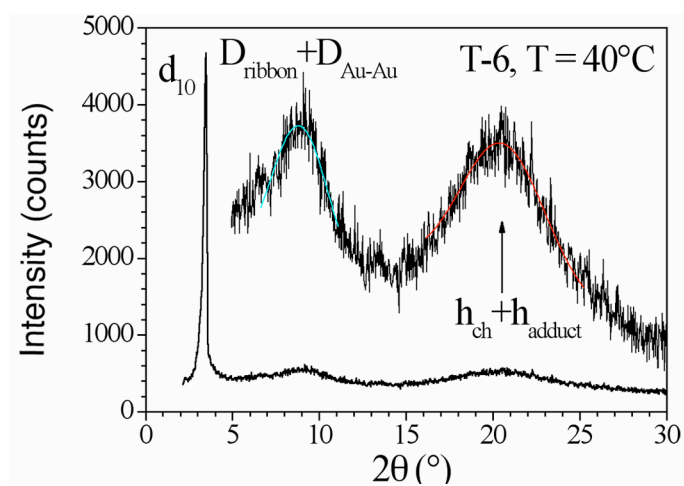
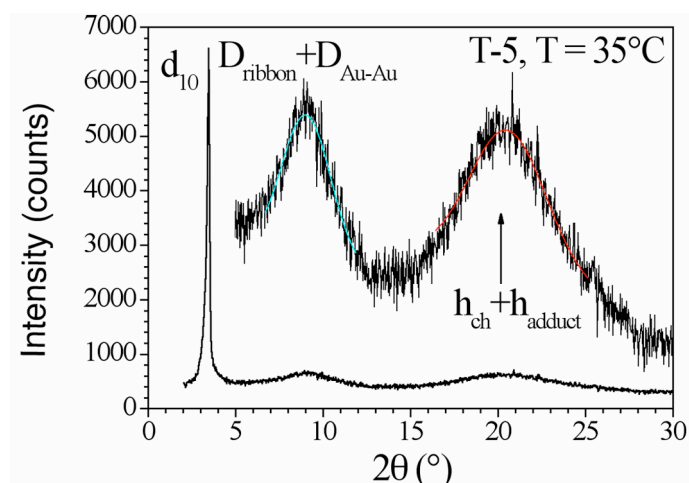
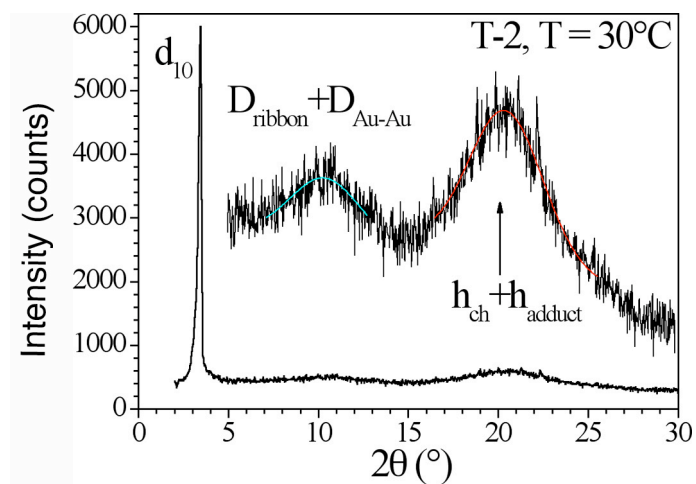


Figure S5. X-ray diffraction patterns of *para* derivatives T-2 (PPh₃), and T-5 and T-6 (BINAP).

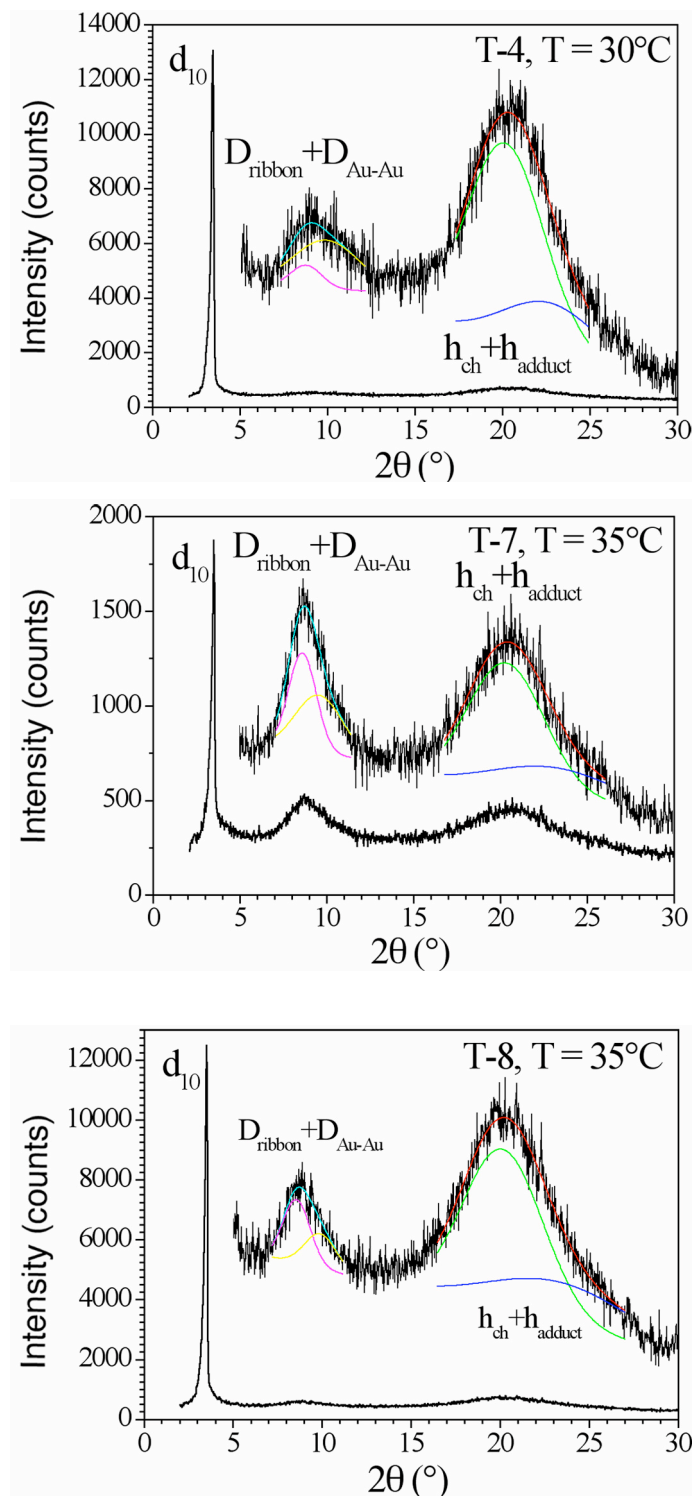


Figure S6. X-ray diffraction patterns of *ortho* derivatives T-4 (PPh₃), and T-7 and T-8 (BINAP).